2. TOKAMAK ISTTOK

J.A.C. Cabral and C.A.F. Varandas (Heads) H. Fernandes, I. Nedzelskij, V. Plyusnin, C. Silva,

M.P. Alonso, B.B. Carvalho, H. Figueiredo, R. Gomes, A. Soares, Y. Tashev

2.1. INTRODUCTION

The activity of this Project in 2002 was mainly focussed on five research lines:

- Testing of the liquid metal limiter concept;
- Diagnostics;
- Slow control system;
- Real-time plasma control system;
- Plasma physics studies.

2.2. TESTING OF THE LIQUID METAL LIMITER CONCEPT[1]

2.2.1. Main activities

The following main tasks were performed in 2002:

- Collaboration with the Association EURATOM /University of Latvia (UoL) on the elaboration of the proposal submitted to CCE-FU for the award of preferential support;
- Collaboration with UoL on the definition of the technical characteristics of the vacuum system;
- Design of a new spectrometer;
- Conceptual study of a combined mass-energy analyser for study of the SOL plasma;
- Participation in meetings in Riga and Princeton about the use of liquid metals in fusion devices;
- Beginning of the elaboration of a review on the use of liquid metals in fusion devices.

2.2.2. Design of a new spectrometer

A new spectrometer is being developed aiming at measuring the liquid metal erosion rate, by means of the determination of Gallium absolute density radial profiles. Its design (Figure 2.1) is based on a 0.5 m imaging, flat field spectrograph with optical fiber transmission for an easier alignment of the experiment. Interchangeable slits allow the use of a CCD multichannel analyzer and photomultiplier tubes as detection systems. This last detector permits to perform time resolved analysis of the Ga impurity content due to the plasma-limiter interaction.
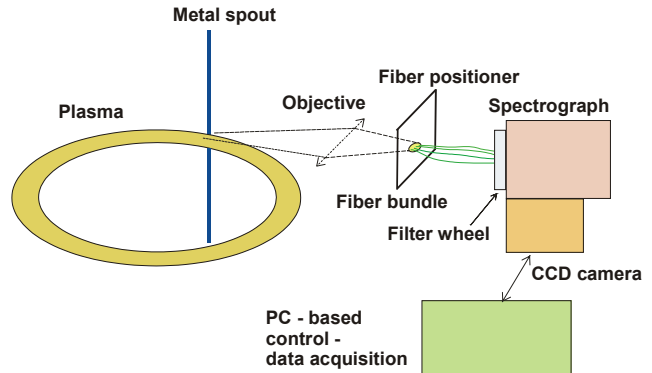
---

[1] Work carried out in collaboration with the Association EURATOM/University of Latvia.

Figure 2.1 - Schematic drawing of the spectrometer to study the plasma-jet interaction

2.2.3. Conceptual study of a combined mass-energy analyzer for the investigation of scrape-of-layer (SOL) plasmas.

The conceptual study of a combined mass-energy analyzer for the investigation of scrape-of-layer (SOL) plasmas was initiated by planning experiments with a liquid metal limiter (LL) on the tokamak ISTTOK.

Traditional spectroscopic impurity diagnostics allow to observe the spatial distribution of high charge state impurities in the main plasma, and the influx of low charge states near the boundary. However, interpretation of the spectroscopic data can be complex and requires additional information. It is also difficult to observe high charge state ions near the plasma edge where the electron temperature and hence the excitation rates are extremely low. Besides, it is well known that impurity transport strongly depends on the background properties of the SOL plasma. Although different types of probes have been developed and effectively used in the investigations of the boundary plasma, till now quite rare data exists, and very limited diagnostic techniques are available for the study of the flux and the charge state distribution of impurities and plasma ions in the scrape-off-layer.

A new diagnostic technique for mass-energy analysis of the SOL plasma and the specification of the operational conditions of the liquid metal limiter have been elaborated. The proposed technique is based on a Bennett-

type mass-spectrometer (BTMS), which generally utilizes the principles of both radio-frequency (RF) time-of-flight mass spectrometer (TOF) and retarding field energy analyzer (RFA). Such a double feature of BTMS gives an additional idea to consider the possibility of its operation in the SOL plasma as a combined mass-energy analyzer.

A simple and inexpensive prototype of the BTMS-RFA is considered for manufacturing and tests using the injector of the ISTTOK Heavy Ion Beam Diagnostic (HIBD).

2.3. DIAGNOSTICS

2.3.1. Main activities

The following main activities were carried out in 2002:

- Maintenance and improvement of the visible spectrometer for the monitoring of the plasma impurities spectroscopic lines;
- Development of a new H_α-diagnostic for the analysis of the light produced by the limiter-plasma interaction;
- Installation, test and operation on ISTTOK of a new injector of the HIBD;
- Development of a 4 channel time-of-flight energy analyzer for the HIBD;
- Optimization of the plasma potential measurements by the HIBD;
- Implementation on ISTTOK of a new set of emissive probes[2], including the development of the dedicated electronics;
- Implementation of a bolometer on the tokamak;
- Remote collaboration on the development of a new Thomson scattering diagnostic for the tokamak GLOBUS-M (S. Petersburg);
- Collaboration on the conceptual design of a new multiplexed Thomson scattering diagnostic for ETE, a spherical tokamak located in S. José dos Campos, Brazil.

2.3.2. H_α diagnostic for monitoring the plasma limiter interaction

A simple diagnostic to measure the light emitted by the limiter-plasma interaction was developed. The H_α–emission line was chosen because it is the strongest one emitted by the hydrogen. The limiter surface is viewed through a normalized vacuum window made of BK7 glass. The emitted light is collimated by a 10 mm diameter lens and focussed to an optical fiber with a diameter of 100 μm. In the other end of the fiber there is a second lens that collimates the light emitted by the fiber and a H_α interference filter. The H_α light is focused by one small aspheric lens to the active area of a Si avalanche photodiode. The electrical signal is provided to an analog-to-digital converter with 1 μs time resolution.
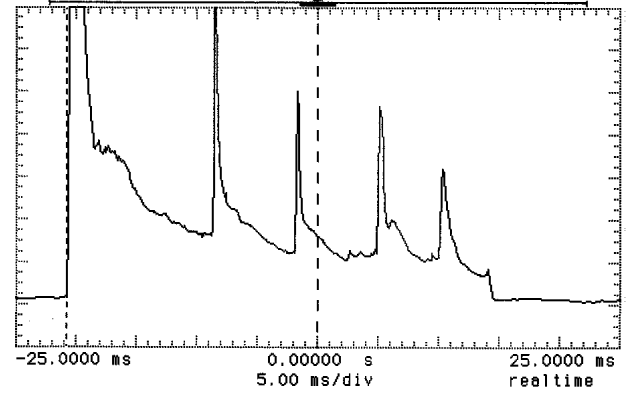

Figure 2.2 – Experimental result

2.3.3. High dispersion spectrometer

Final calibration of the ISTTOK high dispersion spectrometer was performed at 4650 Å (C^{III} spectral line). The apparatus parameters were experimentally determined: the achieved linear dispersion was 1.65 Å/mm. A quartz window was installed on a port allowing the observation of the plasma along a tangential viewing direction. The alignment of this line was made in order to allow measurements of the poloidal velocities. The diagnostic was operated during an ISTTOK campaign. Temporal data has been obtained for both the ion temperature and the plasma poloidal velocity, at the plasma edge region (Figure 2.3).

2.3.4. Elaboration, design and arrangement of four-channel time-of-flight energy analyzer for the heavy ion beam diagnostic

Time-of-flight measurements of the plasma potential by the HIBD with a multiple cell array detector (MCAD) can be generally performed by three schemes shown in Figure 2.4.

The simplest "integral" scheme is the measurement of the average plasma potential by the primary ion beam. The time-of-flight of the ion across the volume with a given distribution of the electrostatic potential ($\Phi(l_{tr}/L_{pl})$) along of the beam trajectory (l_{tr}) is given by the path integral:

$$t_{TOF} = t_{TOFmd}(\Phi=0)(L_{pl}/L_{TOFmd})\{(1/2)\times$$
$$\times \int [q\Phi(l_{tr}/L_{pl})/E_0]d(l_{tr}/L_{pl})+1\}, \qquad (2.1)$$

with ($E_0 \gg q\Phi_{max}$) and where t_{TOFmd} is the time-of-flight from the modulator to the detector, L_{pl} is the plasma dimension, E_0 is the initial energy and q is the charge of the ion.

---

[2] Work performed in collaboration with the University of Innsbruck, on behalf of the Association EURATOM/OÄW.
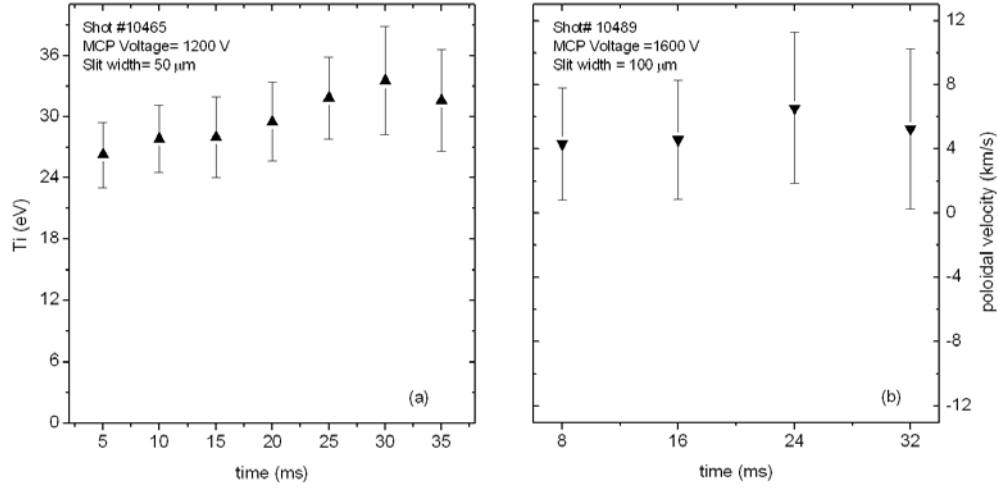
Figure 2.3 - Temporal evolution of the ion temperature and poloidal velocities measurements obtained from ISTTOK's high dispersion spectrometer data analysis.
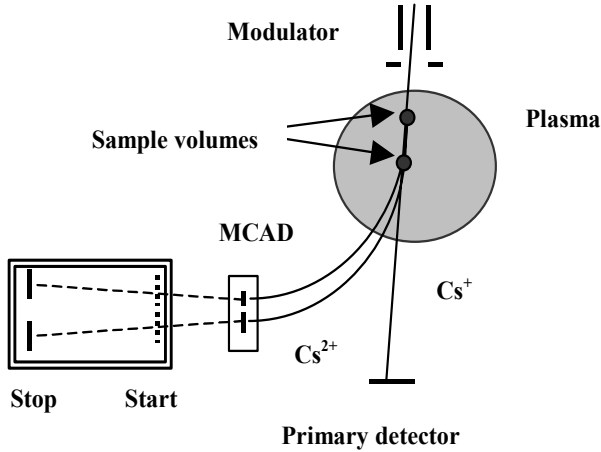

Figure 2.4 - Schematic of TOF measurements of the plasma potential by the HIBD

In the second "quasi-local" scheme the potential drop ($\Delta\Phi(\Delta l_{tr})$) between neighbouring sample volumes inside the plasma can be obtained by measuring the relative time-of-flight of the secondary ions between the respective (effectively "start"-"stop") MCAD cells. The relation for the plasma potential drop is:

$$\Delta t_{TOF} = t_{TOFsd}(\Phi=0)\{(1/2)[q\Delta\Phi(\Delta l_{tr})/E_0]+1\} + \Delta t_{tint}, \qquad (2.2)$$

with $E_o >> q\Delta\Phi$ and where t_{TOFsd} is the time-of-flight of a secondary ion from the sample volume to the MCAD. The term Δt_{tint} is some path integral which for ISTTOK

HIBD geometry can be as low as 10%, depending on the measurement resolution.

The third "local" scheme presents a conventional HIBD measurements of absolute plasma potential ($\Phi(l_{tr})$) and is given by:

$$t_{TOF} = t_{TOFss}(\Phi=0)\{(1/2)[\Phi(l_{tr})/E_0]+1\} \qquad (2.3)$$

with $E_0 >> q\Phi$ and where t_{TOFss} is the "pure" (i.e. with zero plasma potential) time-of-flight between "start" and "stop" detectors arranged along secondary ion trajectories outside the plasma.

The measurements of the changes of the average the plasma potential during minor disruptions of ISTTOK plasmas have been performed successfully. However, the initial experiments with TOF measurements of the plasma potential drop between neighbouring sample volumes have shown that, although the primary beam intensity has been increased 5 times with the new beam injection system, a signal-to-noise ratio for the secondary beam is still too low mainly due to the plasma loading effect.

Figure 2.5 presents a schematic of the four-channel time-of-flight energy analyser (TOFEA) with cylindrical electrostatic steering plates elaborated in CFN for the absolute measurements of the plasma potential. Such a design is minimally influenced by plasma loading and presents the only possibility suited to the severe mechanical constrains of the ISTTOK diagnostic port. Additional conventional electrostatic plates are foreseen for a careful beam alignment. The "start" (mesh) and "stop" (plate) detectors of the TOFEA are arranged inside double-shielded boxes to minimize the electrically coupled and electromagnetic interference noise.
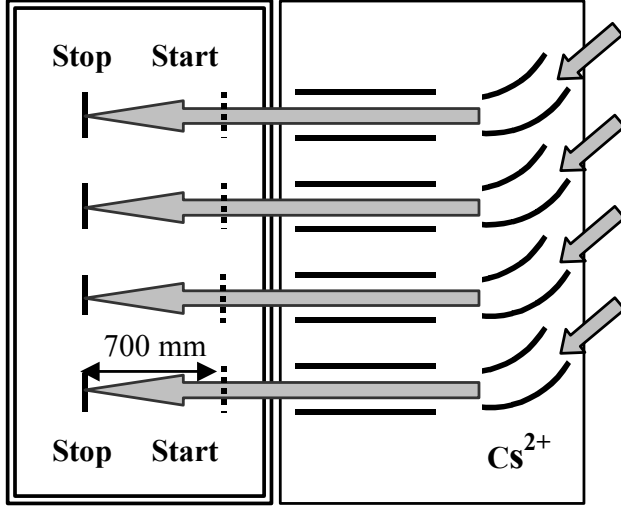
Figure 2.5 - Four-channel TOFEA

2.3.5. Bolometer

A bolometer has been installed on ISTTOK to evaluate the time evolution of the radiation losses. The diagnostic is based on photodiodes produced by International Radiation Detectors (IRD), which are characterized by a flat spectral sensitivity and by a high temporal resolution. Two different detectors have been installed corresponding to different energies sensitivities: (i) AXUV, from soft X-rays to ultra-violet radiation; and (ii) UVG, from ultra-violet to visible radiation. The photodiodes are operated in unbiased mode and without preamplifiers. Figure 2.6 shows the time evolution of the bolometer signals together with the line-averaged density for a discharge with electrode biasing. As expected the time evolution of the radiation losses follows that of the density. It is also clear that time evolution of the signals from both detectors is very similar, indicating that ultra-violet radiation is dominant on ISTTOK (both detectors are sensitive to that spectrum region).

2.3.6. Evaluation of the incident angle of the beam into a 30° electrostatic energy analyzer of a heavy ion beam probe (HIBP)

The resolution of the plasma potential measurements by a 30° electrostatic energy analyzer of a HIBP is strongly related to the accuracy of the knowledge of the incident angle of the beam (θ). Initially it is determined by the calculations of the beam trajectories in the confining magnetic field of the plasma device. However, because the magnetic field simulation codes are not exact, an uncertainty in θ always exists. A common practice to reduce the influence of this uncertainty consists in tuning the analyzer geometry parameters aiming at minimizing the dependence on θ resulting from a scan of the beam across the plasma. Still, the attachment of the energy analyzer to the diagnostic port cannot be controlled with enough

precision and, therefore, an unknown shift from the chosen optimal range of θ is predictable.

A method for the direct evaluation of the incident angles during operation of a HIBP on plasma experiments has been proposed. It is based on the addition of a second split-plate detector along a 30° exit axis of the analyzer, and on the comparison of the respective normalized beam currents. With these two detectors the incident angle of the beam into the analyzer (θ) is determined by a simple relation:

$$\text{tg}\theta = [(2l/w + \Delta i)/(2l/w - \Delta i)]\text{tg}30° \qquad (2.4)$$

where l is the extension length between two detectors, w is the width of the analyzer incident slit, and Δi is the difference of the normalized currents of the two detectors.
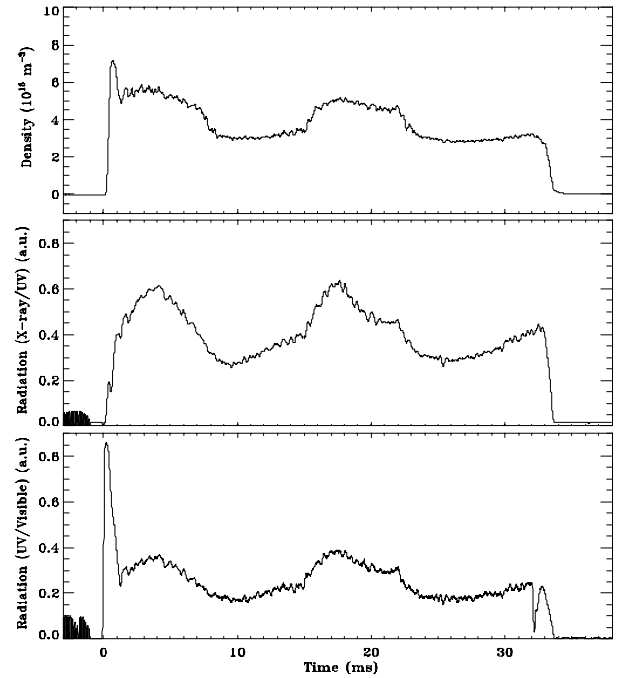

Figure 2.6 - Time evolution of the line–averaged density together with the radiation losses measured by X-rays/UV and UV/visible detectors.

The experimental verification of the method has been performed on the HIBP test facility of the Institute of Plasma Physics (Kharkov, Ukraine). Figure 2.7 presents the experimental results of the evaluation of the entrance angle θ in the full dynamic range of ΔI as a function of U_b/U_a, the ratio of the acceleration and analyzer voltages. Figure 2.8 demonstrates that an accuracy better than $\Delta\theta = 0.1°$ can be attained.

This method is considered for the implementation in a new 30° electrostatic energy analyzer designed for the HIBD of the T-10 tokamak, of the "Kurchatov Institute" (Moscow, Russia).
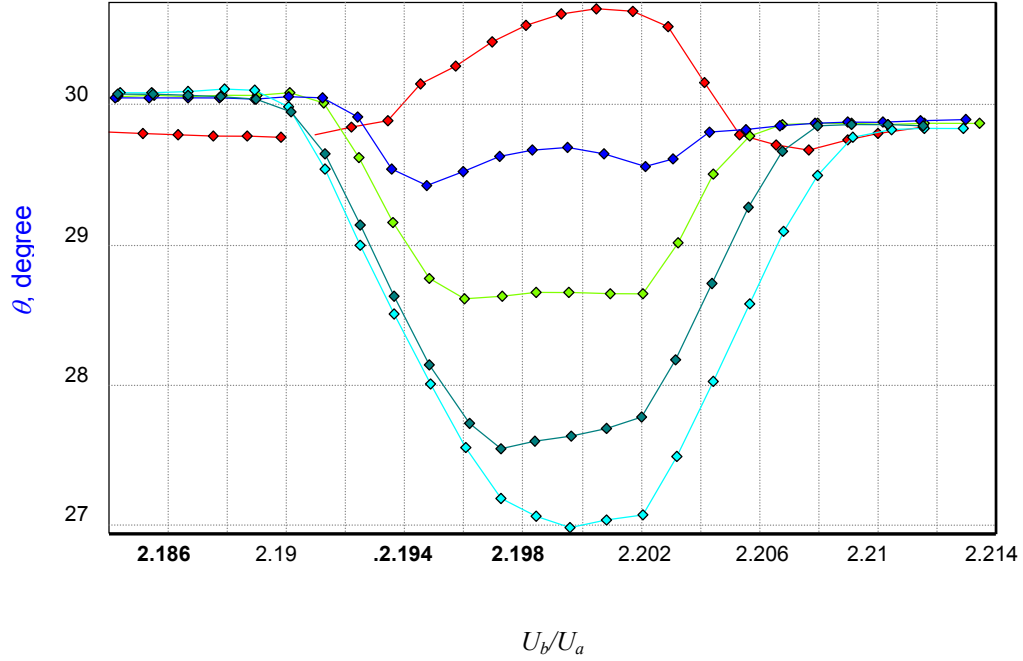
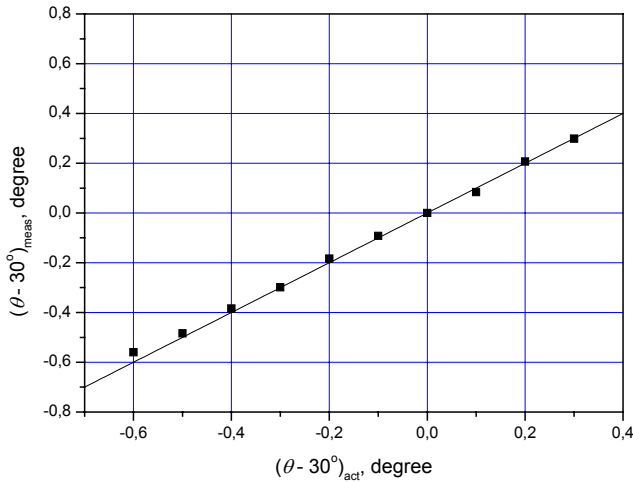Figure 2.7 - Experimental results of the evaluation of the entrance angle θ in the full dynamic range of Δi.

Figure 2.8 - Measured (θ - 30º)_meas versus actual (θ - 30º)_act demonstrating the accuracy of the method.

2.3.7. Multipoint Thomson scattering diagnostic for the ETE tokamak

A Multipoint Thomson Scattering (MTS) diagnostic based on time-delay techniques is being developed in collaboration with "Instituto Nacional de Pesquisas Espaciais" (Brazil) to upgrade the present ETE Thomson scattering diagnostic.

Figure 2.9 shows a schematic view of this diagnostic. The MTS time-delay results from the use of several optical fibers with different lengths to relay the light signals from a plasma-laser chord to a single polychromator. The diagnostic will allow simultaneous measurements at twenty spatial plasma positions with a resolution of 25 mm. The estimated difference on the fiber lengths is about 14 m.

The MTS is based on a 10 J Q-switched ruby laser (λ = 694.3 nm, pulse duration: 30 ns) that probes the plasma horizontally at the mid-plane. A f/6.3 lens images the scattered light into an optical fiber bundle that is further spectral analyzed by a 5-channel filter polychromator.

 About 3×10^5 scattered photons are expected in a solid angle of 2.69×10^{-2} sr assuming the ETE plasma parameters (T_e = 160 eV and $n_e = 2\times10^{19}$ m^{-3}) and limiting the laser energy to 4 J. This means that 2×10^4 incident photons are expected on the silicon avalanche photo detector in any first spectral channel. The total transmission of the system is expected to be 52% for fibers with an attenuation of 2 db/km.

2.4. SLOW CONTROL SYSTEM
2.4.1. Introduction
The control of the ISTTOK operation has been performed by a computerized system based on a commercial vacuum controller unit (slow control) and an on-site developed VME timing unit (fast control).
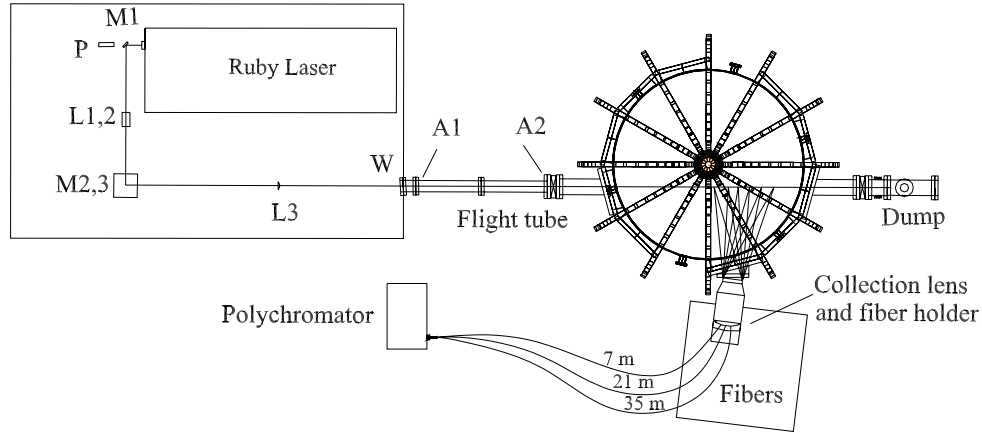
19

Figure 2.9 – Proposed Multipoint Thomson scattering for the ETE tokamak: M1,2,3: flat mirrors; P: photodiodo; L1,2: beam expander; L3: 3 m focusing lens; W: entrance window; and A1,2: apertures.

In order to overcome some constraints of the vacuum controller unit (EDWARDS 2032), a new slow control system has been developed by CFN staff. The following main activities were carried out in 2002:

- Finalization of the assembly and testing of the hardware modules;
- Finalization of the development of the software;
- Testing of the slow control system.

2.4.2. Description of the new slow control system

The new slow control system (Figure 2.10), designed in a hierarchical structure, is composed by a supervisory unit (US), several distributed control units (UCD) dedicated to the ISTTOK subsystems and a commercial vacuum monitor unit (PFEIFFER Maxi-Gauge), connected by a robust open fieldbus standard (CANbus ISO 11898/11519). The supervisory unit, based on a personal computer (Pentium IV, 1GHz, 512 kB RAM), monitors the entire plant operation and serves as the operator console.
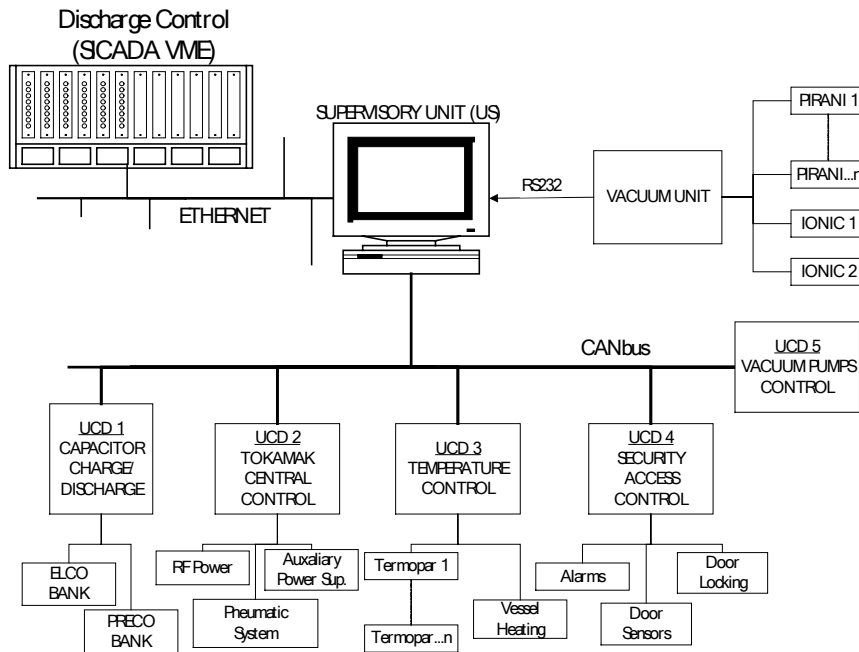

Figure 2.10 - A new ISTTOK slow control schematic configuration

20

The distributed control units (Figure 2.11) are embedded modules build in Eurocard 3U format cards and installed in 19" racks. These modules have been on-site developed, based on low cost 8 bit microcontrollers (PIC16F876) running at 20 MHz. CANbus connectivity is performed by a dedicated controller circuit (MCP2510). Each module has an analogue input/output section configured to the needs of each subsystem. This section can have analog-to-digital and digital-to-analog converters, relay outputs and electrical or optical digital inputs. The control modules can be extended to other extra microcontroller through an I^2C connection.

The control software system has been developed on a distributed, decentralized, object-oriented and modular philosophy (Figure 2.12). Operator graphical user interface (GUI), plant monitoring and supervising, data storing and operational mode transition are made by the supervisory unit. Real-time control, cyclic signal measuring, and security tasks are executed by the distributed units. A network application running on a HTTPD server enables INTERNET users to monitor ISTTOK status. Another SSL secured application permits the operator to remote control selected subsystems (vacuum, discharge cleaning, etc).

2.5. REAL-TIME PLASMA CONTROL SYSTEM
2.5.1. Main activities
The following main activities were carried out in 2002:
- Development of the feedback control systems of the primary current and vertical magnetic field;
- Development of a SQL database for the experimental results;
- External calibration of the magnetic probes and of the acquisition system;
- Development of numerical codes for signal analysis and algorithms for the control of the plasma position;
- Development of tools for the remote access to the experimental results;
- Test of the performance and accuracy of the system.

2.5.2. Testing of the real-time plasma control system
2.5.2.1. Introduction
A real-time MHD diagnostic for feedback plasma control has been installed in ISTTOK as a new node of the control and data acquisition system (SICADA). The final configuration of the hardware system is depicted in Figure 2.13 and is described in detail in the "2001 Annual Report".
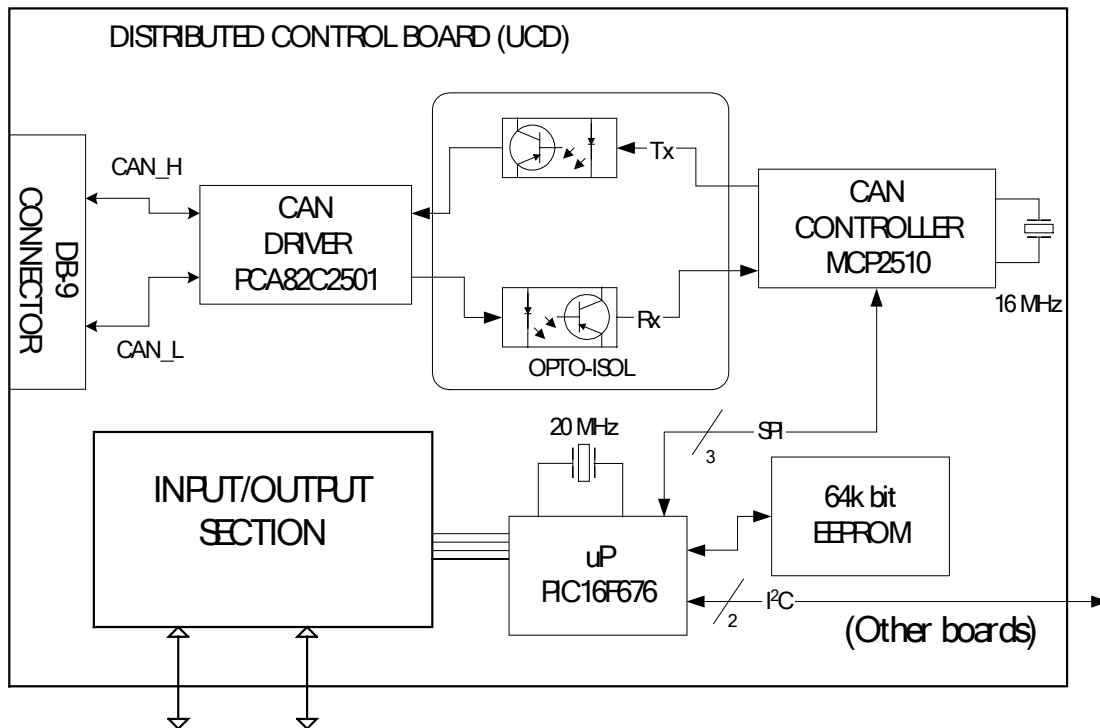

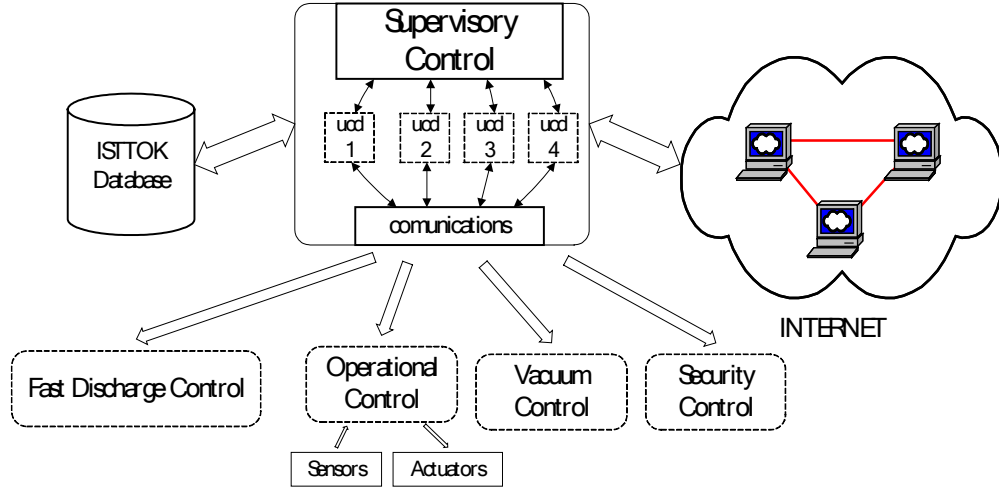*Figure 2.11 - Block diagram of the distributed control module*

Figure 2.12 – Block diagram of the software of the ISTTOK new slow control system

2.5.2.2. Algorithm for real-time plasma control

An algorithm was developed for real time-plasma control. The plasma current was modelled by a finite set of current filaments:

$$j\psi = \sum_{n=1}^{N} \delta(r - r_n, z - z_n)I_n \qquad (2.5)$$

where the coefficients I_n and the filament coordinates (r_n, z_n) are obtained by a least squares method, minimizing the error of the estimated poloidal magnetic fields to the measured signals by twelve probes covering one poloidal section. These coefficients are used to determinate the displacements of the current distribution. The plasma boundary is estimated by the first magnetic poloidal isoflux line that touches the limiter or the inner vessel. These calculations are performed in real-time (each *1 ms* cycle) by a Digital Signal Processor (DSP).

The displacement of the plasma column is compared with reference values and applied to a feedback control routine which generates a digitally controlled Pulse Width Modulation pattern (Figure 2.14). The transformer primary current and the poloidal external equilibrium magnetic fields are finally controlled, using insulated gate bipolar transistors (IGBT) driven by these PWM patterns at a 5 kHz rate.

The overall performance and accuracy of the system were already evaluated. Figure 2.15 shows the evolutions of the axis of the plasma current and of the average plasma density measured by the microwave interferometer. Analysis of this figure allows to conclude that axial offsets of the plasma current occur when there are pseudo-falls of the average plasma density.
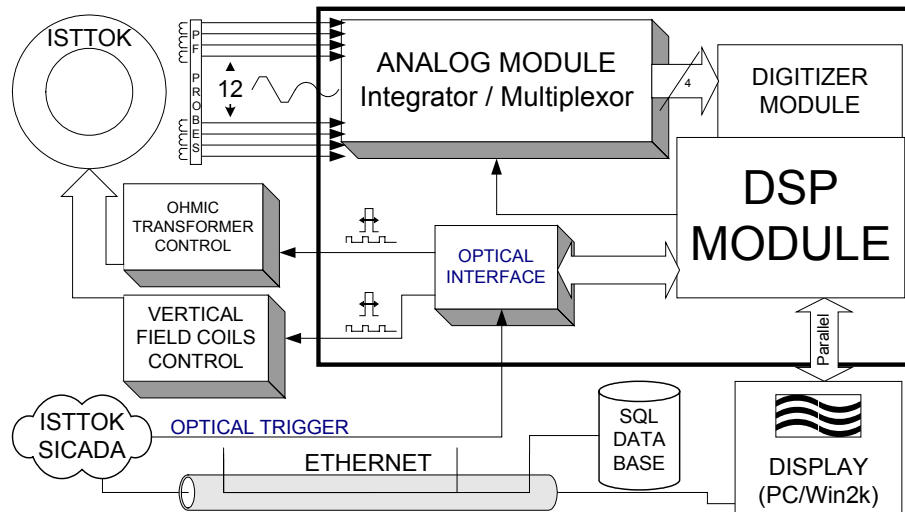

Figure 2.13 - Configuration of the MHD diagnostic for real-time control of ISTTOK operation.
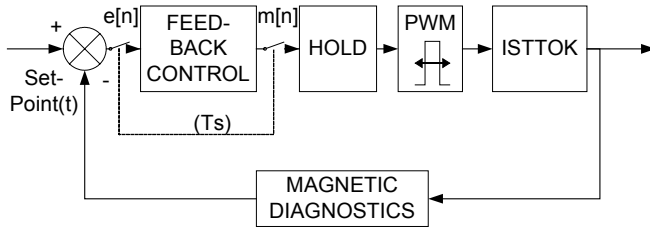
Figure 2.14 - Feedback control diagram

2.5.2.3. Laboratorial tests

Intensive tests have been carried out in the laboratory for the calibration of this new diagnostic as well as for testing of the signal analysis codes and algorithms for the determination of the plasma column position.

Figure 2.16 shows the experimental set-up used in the laboratory tests and the results calculated with the numerical codes. Analysis of this figure allows to conclude that the results provide by this diagnostic have a good accuracy with the real location of the axis of the test current.

2.5.2.4. Web-browser software interface

A new SQL database compatible with the older data-shot structure have been implemented, being the corresponding data migration schedule for 2003 as soon as all data retrieve software tests have been accomplished. Some data is already available throughout the new data-mining internet-browser concept (Figure 2.17).

2.6. PLASMA PHYSICS STUDIES
2.6.1. Introduction

The following Plasma Physics studies were carried out in 2002:

- Investigation of the runaway electrons (RAE) characteristics in discharges with minor and major disruption events;
- DC electrode biasing experiments;
- Simultaneous limiter and electrode biasing experiments;
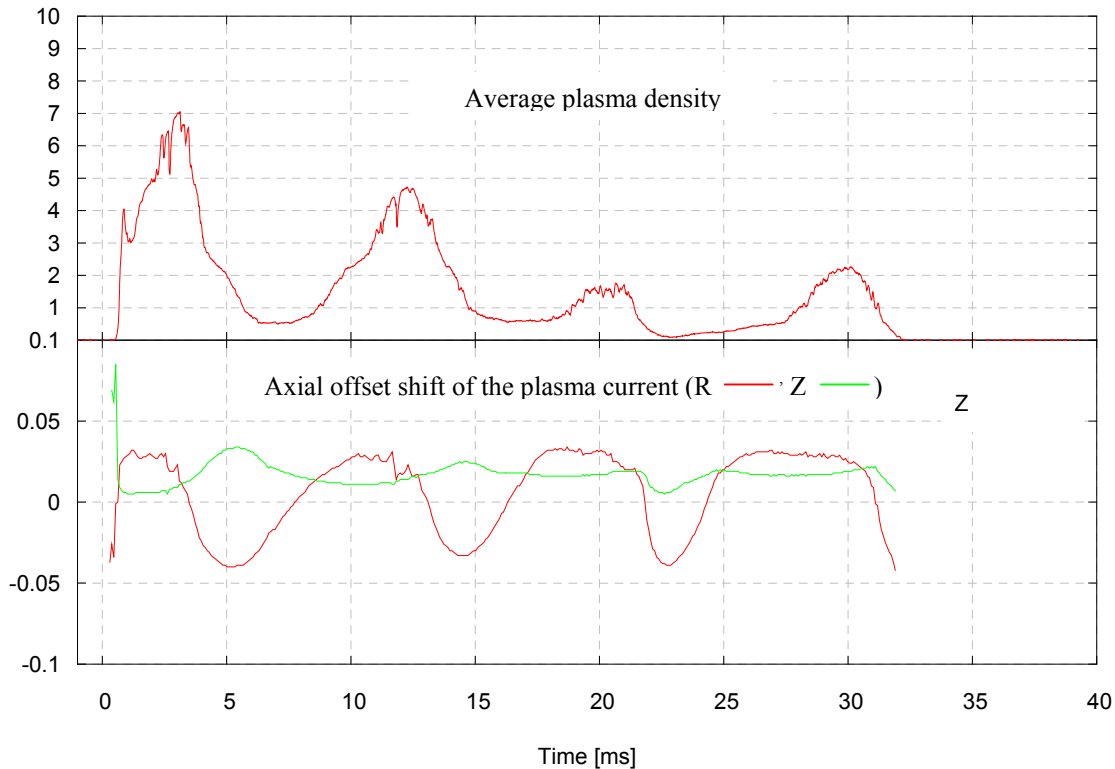- Measurement of the plasma potential by emissive probes.

Figure 2.15 – The axial offset shift of the plasma current, measured by the new set of magnetic probes, and the corresponding pseudo-fall of the plasma density due to the associated plasma column shift from the interferometer measuring chord.
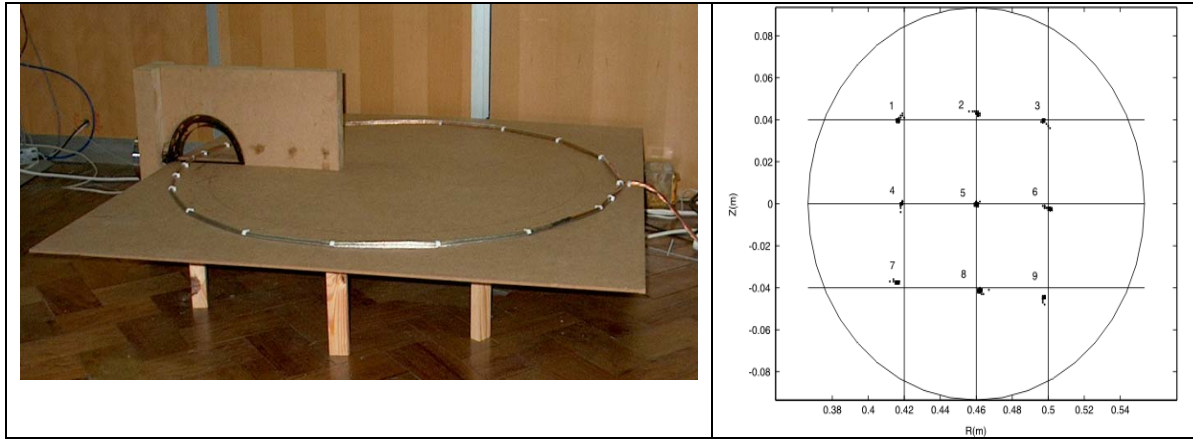
23

Figure 2.16 – Magnetic probe calibration carried out by different current loops arrangements.
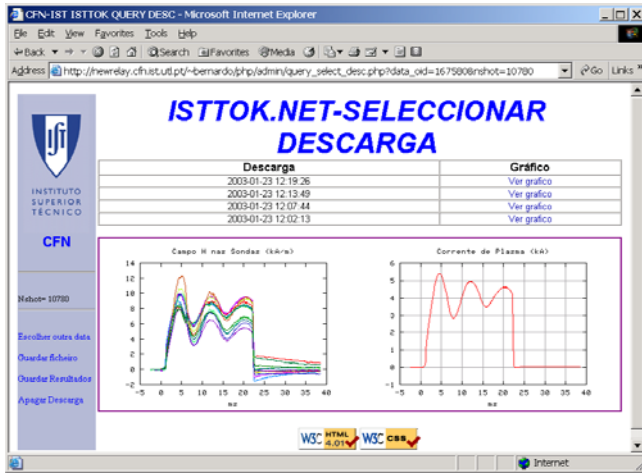

Figure 2.17 – The new web-browser software interface for data mining allowing a fast data interest recognition and retrieve.

2.6.2. Investigation of the runaway electron characteristics in discharges with minor and major disruption events

Evolution of the plasma parameters in discharges with RAEs and disruptive events has been analysed using the self-consistent numerical model, which includes the calculations of the plasma power-energy balance and the determination of the runaway process characteristics, such as runaway electron current (I_{RA}), density (n_{RA}) and energy (W_{RA}).

The sequence of measured and numerically modelled events in the discharge #8400 (Figure 2.18) is in adequate agreement with the temporal evolution of the discharge image obtained using the soft X-ray diagnostic (Figure 2.19). In the first stage of the implementation of this diagnostic on ISTTOK, the 9-channel system was used for the measurements of spatial and time variations of the soft X-ray emission in the energy range 1-20 keV. Comparison of the contour plot of the emission structure with the evolution of the loop voltage signal (V_{loop}) reveals obvious coincidence between the broadening of the soft X-ray emission profile (near the plasma periphery) and the regular spikes in V_{loop}, which appeared due to the runaway instability (between 0.025 s and 0.026 s in Figure 2.19). During the same time, just prior to the minor disruption (t = 0.0261 s), the helical perturbations of the central part of the plasma caused by the MHD activity are clearly distinguished in the soft X-ray image. A similar coincidence between the broadening of the soft X-ray emission profile (now it develops from the plasma core) and V_{loop} spikes is also clearly seen between 0.027 s and 0.028 s. The increase of the transverse energy of the plasma electrons during the instability causes this broadening of the soft X-ray emission profile, since the plasma density does not change significantly. Analysis of the emission structure during minor (t=0.0261 s) and major (t=0.0292 s) disruptions (Figure 2.19) enabled to determine the most probable locations, where the RAEs interact with the surrounding plasma surfaces. These zones are detected as spots of the soft X-ray emission on the top and bottom parts of the plasma column. The energy of the RAEs at which they hit the wall was estimated by a numerical analysis (Figure 2.18).

The developed algorithm of the experimental data analysis was investigated concerning its possible use for the modelling of the runaway generation during a thermal quench in large-scale tokamak disruptions. Calculations performed in frames of the simplest model of the single test particle acceleration and 0-D calculations of the runaway density predict a strong increase of the longitudinal electric field and the creation of RAEs with substantial energy and density due to the Dreicer mechanism for the case of 1 keV thermal quench in a
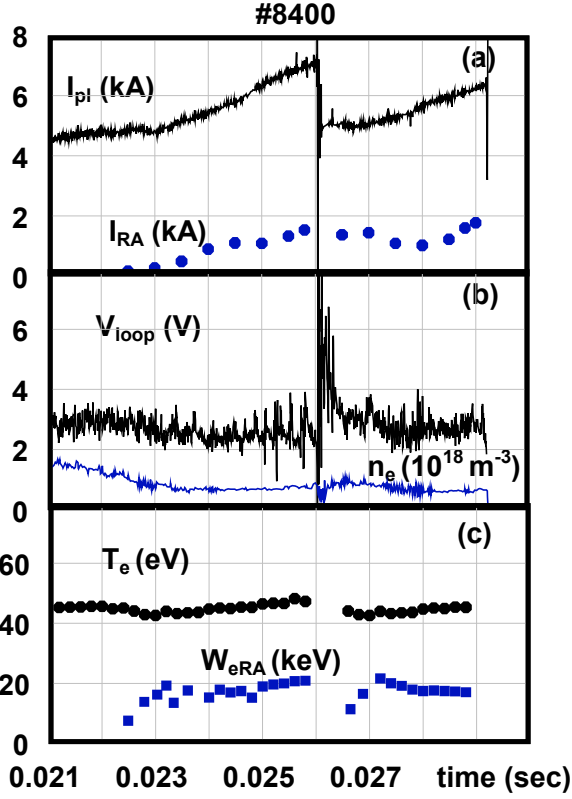
#8400

Figure 2.18 - *Evolution of the plasma parameters in discharge #8400 with runaway generation and minor and major disruptions. The average electron temperature T_e was calculated by the power-energy balance. W_{eRA} estimated runaway electron energy*

Contour plot of the soft X-ray image of shot #8400

Figure 2.19 - *Soft X-ray image of the discharge #8400. The partial disruption is observed at t=0.026 sec. Discharge is finalized by the major disruption. The zones where energetic electrons hit the plasma surrounding surfaces are clearly highlighted on the top and bottom of the plasma column. Runaway instability is identified in a kind of closely coincided bursts of the soft X-rays and loop voltage spikes.*

large-scale tokamak (a_{pl}=1-1.2 m, 2 MA<I_{pl}<6 MA, $\langle n_e \rangle$=10^{20} m^{-3} and temperature decay within 100-500 µs). Analysis of the numerical results shows that runaway electrons increase their energy and density mainly during the stage when electron temperature decreases below 100 eV (Figure 2.20). Duration of this phase has to be considered as the most critical parameter, since even for τ_{fast} ~200 µs, the energy of the runaways can achieve up to 7-10 MeV at a density of ~10^{11}-10^{12} m^{-3}. Creation of runaways with such parameters obviously can cause the process of secondary RAEs avalanche, which leads to an abrupt increase of the RAEs density at an energy exceeding 10 MeV.

2.6.3. Electrode and limiter biasing experiments
2.6.3.1. Introduction
Limiter and electrode biasing experiments have been performed on ISTTOK in order to control the edge radial electric field and to investigate its impact on the plasma confinement. In addition to the constant bias voltages used in most biasing experiments, AC bias has also been investigated on ISTTOK. Two different bias configurations, limiter and electrode, have also been compared in the same device, in particular in what concerns their effects on the edge plasma parameters.
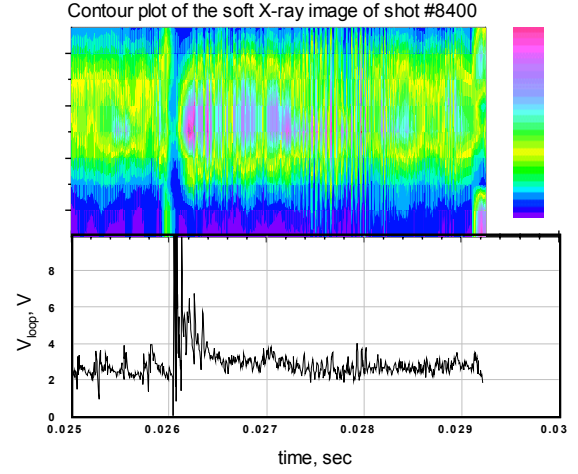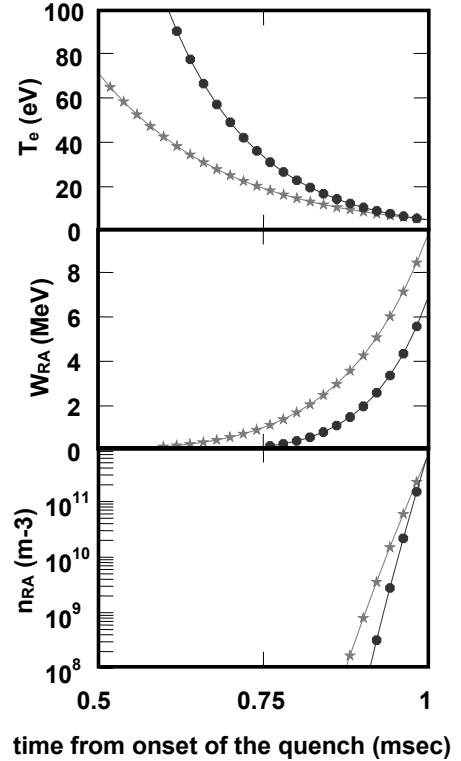

Figure 2.20 - *Modelling of runaway generation during a thermal quench in a large-scale tokamak disruption (a_{pl}=1 m, I_{pl}=2.5 MA, n_e=10^{20} m^{-3}). Runaway energy (W_{RA}) and density (n_{RA}) calculated for two values of the pre-disruptive electron temperature: T_e=1 keV (stars) and T_e=10 keV (circles). In both cases the electron temperature decays to 5 eV within 1 ms.*

2.6.3.2. Electrode biasing (EB)

The time evolution of the main plasma parameters for a discharge with constant electrode bias (V_{bias}=+100 V) is presented in Figure 2.21. The shadowed area indicates the time when the bias is applied. An unbiased discharge is also shown for comparison. The most striking change in the core parameters as a result of positive EB biasing is the large increase in the line-averaged density (~ 40%). A small drop in the plasma current (~ 10%) is observed, which is possibly a consequence of the plasma cooling induced by the increase on the radiation losses. Contrary to the density, both the plasma current and the temperature start to change only ~1 ms after the bias is applied and then slowly decrease. For that reason the plasma stored energy increases significantly when the bias is applied and starts to decrease slowly a few milliseconds later.
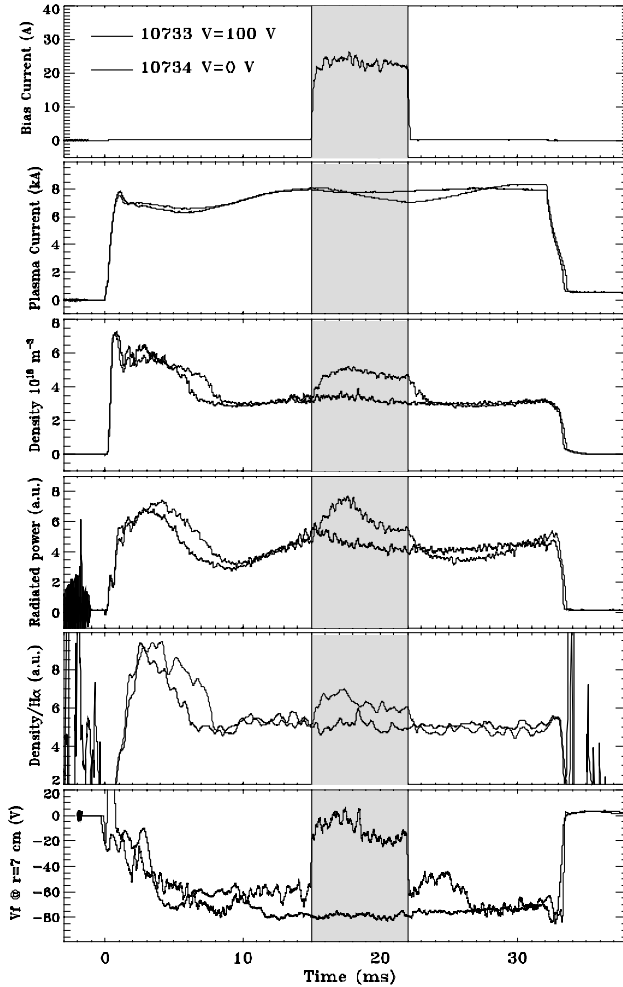

Figure 2.21 – Time evolution of the main plasma parameters for a discharge with DC electrode bias (V_{bias}=100 V). The shadowed area indicates the time when the bias is applied. A discharge with no applied voltage is also shown for comparison.

Changes in the gross global particle confinement time (τ_p), are inferred from the ratio of the line-averaged density to the H_α intensity, which is a rough estimation of τ_p. Although both n_e and H_α radiation increase, a clear enhancement in gross confinement (n_e/H_α) (~ 20%) is observed. This result is corroborated by probe measurements, which show a decrease in turbulent particle transport when the bias is applied.

For positive EB, the floating potential in the plasma edge is modified in a fast time scale (<100 μs). For the discharge shown in Figure 2.21, the floating potential at the electrode position increases by ~50 V, while close to the limiter does not change significantly, leading to an increase in the edge radial electric field (from 2 to 6 kV/m) in the region just inside the limiter. This modification in the edge E_r profile may explain the observed reduction in turbulent transport and the improvement in particle confinement.

Turbulent particle transport has been computed from the probe data. The turbulent transport is strongly reduced after the bias is applied, although it increases again when the bias is swished-off. The I_{sat} and V_f fluctuation levels are reduced by a factor of ~2 when positive EB is applied. Spectral analysis of both I_{sat} and V_f signals confirms the reduction on fluctuations, in particular for frequencies between 20 and 80 kHz.

For negative bias (-250<V_{bias}<0 V) no significant modification on the global or edge parameters were observed. The measured electrode current for negative bias the electrode current is very small, ($\leq$ 1 A), which does not seen to be sufficient to modify plasma rotation and therefore change confinement significantly. For negative bias the current is limited by the electrode ion saturation current. A reasonable agreement between the expected and observed ion saturation current to the electrode is found,

$$I_{sat}^{elec} \approx 0.5eSn_e(T/m_i)^{1/2} \approx 0.6 \text{ A} \qquad (2.6)$$

where S is the double cross-section of the collecting part of the electrode.

2.6.3.3. Limiter biasing (LB)

Non-intrusive limiter biasing experiments have been already formerly described in detail. A comparison of the main plasma parameters during DC limiter and electrode bias discharges (V_{bias}=120 V) is presented in Figure 2.22. The time evolution of the main plasma parameters during limiter biasing is similar to that observed in EB experiments. However, the perturbation induced by LB is stronger, as the increase in the radiation losses is larger with LB. Although n_e rises for positive LB, both the H_α radiation and the turbulent particle transport also increase significantly, leading to very limited modifications in particle confinement when the bias is applied and a substantial confinement degradation a few milliseconds later due to a large reduction on the plasma current and
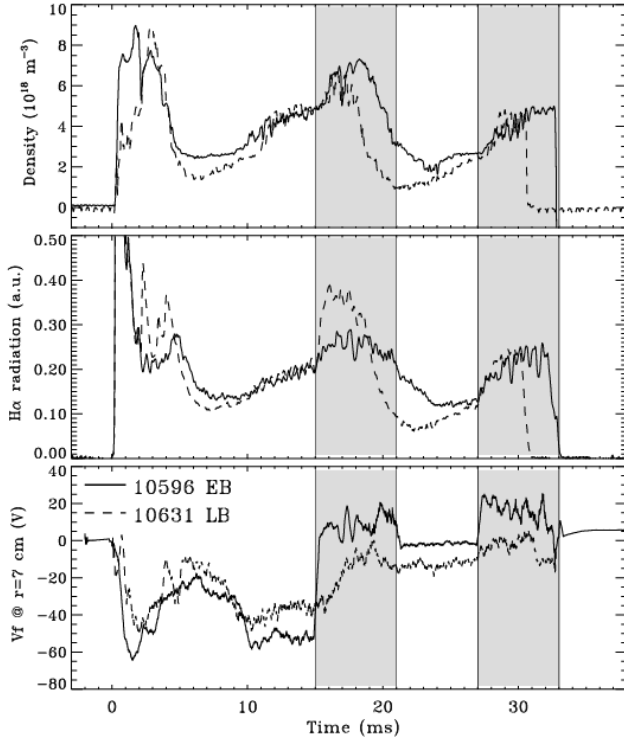
Figure 2.22 - Comparison of the time evolution of the line-averaged density, H_α radiation and floating potential for a discharge with DC electrode bias and another with limiter bias ($V_{bias}=100$ V).

temperature. Results indicate that the increase in density, although in general smaller than that observed with EB, is not a consequence of an improvement in the confinement. The large rise in the H_α radiation after the bias is applied suggests an increase in the plasma fuelling, probably due to the increase in the limiter outgassing resulting from the modification of the plasma-wall interactions.

Analysis of the Langmuir probe data has shown that in the region inside the limiter (r<a) floating potential follows the applied voltage; V_f increases by ~20 V. However, the V_f modification is much smaller than that observed for EB resulting in a modest modification in E_r (~2 kV/m), localized mainly in the SOL. An interesting observation is that the increase in V_f is slower for LB when compared with EB. The maximum floating potential is only reached 2 ms after the bias is applied. This means that when the maximum E_r is attained the radiation losses are already substantial, restricting considerably the effect of E_r on confinement.

2.6.3.4. Simultaneous limiter and electrode biasing

A velocity shear stabilization mechanism has been proposed to be responsible for an improvement in confinement. A clear correlation between reduction of turbulence and the modification of radial electric fields induced by bias was shown in several experiments. The control of the shear layer is therefore an important tool to modify transport in tokamaks. Simultaneous limiter and electrode bias has been used on ISTTOK to investigate the possibility of shaping the plasma potential profile.

Preliminary results show that the control of the V_p profile by simultaneous limiter and electrode bias is very limited. Experiments indented to suppress/reinforce the shear layer, applying voltages with different polarities to the limiter and the electrode, were only partially successful. Experiments show that the plasma potential can be easily increased in the region between the limiter and the electrode with positive bias. In opposition, negative voltages do not modify the plasma parameters, in particular do not affect the V_p profile, strongly limiting therefore the possibility of shaping the shear layer.

2.6.4. Physics studies based on emissive probes[3]

2.6.4.1. Introduction

Recent measurements were performed on ISTTOK with a radially movable arrangement of three emissive probes, positioned in such a way that the radial and the poloidal components of the electric field and their variations in the edge region can be simultaneously recorded (Figure 2.23). For probe 2 (taken as the reference probe) located at the last contour flux surface (LCFS) the radial spacing between probe 1 and both probes 2 and 3 is 7 mm, while probes 2 and 3 are spaced 5.8 mm in the poloidal direction. The movement of the probe array is not performed in the radial direction, therefore the distances between the probes are slightly changed.
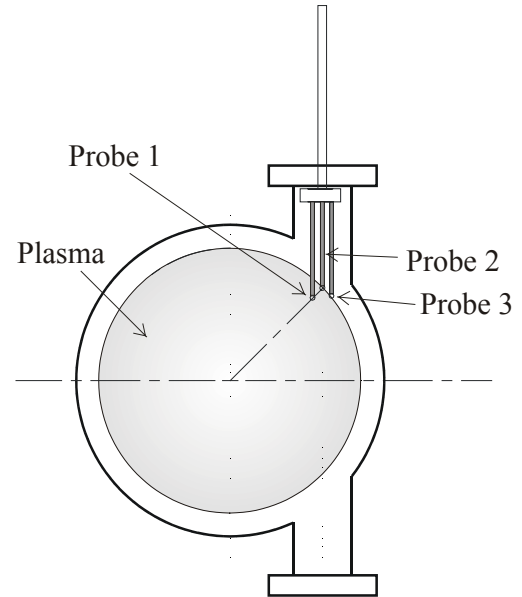

Figure 2.23 – Implementation on ISTTOK of the three emissive probes

---

[3] Work carried out in collaboration with the University of Innsbruck.

2.6.4.2. Plasma potential profiles

Plasma potential profiles were obtained allowing the comparison between biased (130 *V* DC applied to an electrode inserted 1 cm in the plasma) and non-biased plasmas (Figure 2.24).
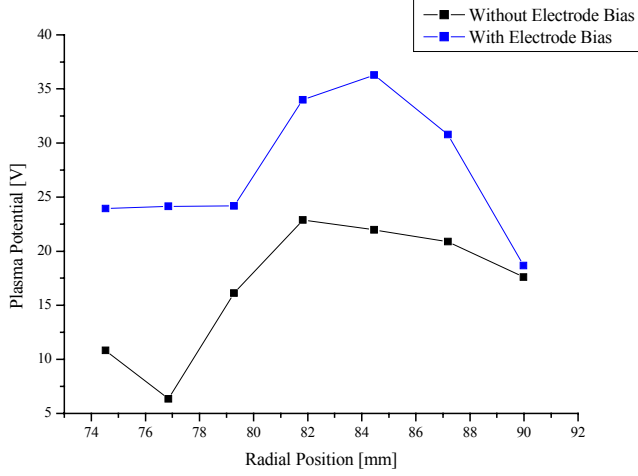

Figure 2.24 – Measurement of the radial profile of the plasma potential without and with electrode biasing

2.6.4.3. Preliminary Reynolds stress measurements

Preliminary measurements with this probe array have up to now delivered the Reynolds stress (Re) in two different positions. In both cases all three emissive probes have been heated so that the plasma potentials $\Phi_{pl,1-3}$ could be determined from the floating potentials of the probes. From these three values,

$$E_r = (\Phi_{pl,1} - \Phi_{pl,2})/d_{12} \tag{2.7}$$

and

$$E_\theta = (\Phi_{pl,3} - \Phi_{pl,2})/d_{23} \tag{2.8}$$

were calculated.

The Reynolds stress, defined as

$$Re = \langle \widetilde{v}_r \widetilde{v}_\theta \rangle \cong \langle \widetilde{E}_r \widetilde{E}_\theta \rangle / B_0^2 \tag{2.9}$$

can be calculated from the above mentioned values. If the Reynolds stress has a gradient, this leads also to an enhanced radial particle flux. Table 2.1 shows a summary of the measurements hitherto and a comparison with former measurement of *Re* in the ISTTOK using cold probes.

Minor radius [mm]	Re [m^2/s^2], determined by means of the three emissive probes heated	Re [m^2/s^2], determined by means of the three emissive probes not heated	Re [m^2/s^2], determined by means of the three cold probes
74,82	-2.3×10^6	-4.9×10^6	$\cong -4\times10^6$
80,32	-0.86×10^6	-4.3×10^6	$\cong 0.5\times10^6$

Table 2.1 – values of the Reynolds stress calculated in ISTTOK plasmas